Artificial Life and Robotics manuscript No.
(will be inserted by the editor)

Quadrupedal Running with a Flexible Torso: Control and Speed Transitions with Sums-of-Squares Verification

Qu Cao · **Ioannis Poulakakis**

Received: date / Accepted: date

Abstract This paper studies quadrupedal bounding in the presence of flexible torso and compliant legs with non-trivial inertia, and it proposes a method for speed transitions by sequentially composing locally stable bounding motions corresponding to different speeds. First, periodic bounding motions are generated simply by positioning the legs during flight via suitable (virtual) holonomic constraints imposed on the leg angles; at this stage, no control effort is developed on the support legs, producing efficient, nearly passive, bounding gaits. The resulting motions are then stabilized by a hybrid control law which coordinates the movement of the torso and legs in continuous time, and updates the leg touchdown angles in an event-based fashion. Finally, through sums-of-squares programming, formally verified estimates of the domain of attraction of stable fixed points are employed to realize stable speed transitions by switching among different bounding gaits in a sequential fashion.

Keywords Quadrupedal bounding · flexible torso · domain of attraction · sums of squares

1 Introduction

Recently, quadrupedal running with flexible torso has received considerable attention in the context of reduced-order models [1, 6, 18, 23], often termed "templates" [7]. As in the Spring Loaded Inverted Pendulum (SLIP) [7], templates for quadrupedal running typically employ massless, springy legs, and were primarily used to establish conditions under which cyclic running motions can be passively generated, through the interaction of the torso oscillations with the leg movements [1]. Echoing the SLIP [7], as well as early rigid-torso bounding models [13, 24], it was found that passively stable bounding can be realized in the presence of torso flexibility [2], provided that the torso flexibility and leg compliance are suitably tuned. Furthermore, by actively coordinating the torso's flexion-extension oscillations with the movement of the legs the capability of the system in dealing with disturbances can be drastically improved [2].

The aforementioned models, however, cannot be directly used to develop control laws for more realistic quadrupedal robot models with non-trivial leg mass, such as those in [5, 11, 14]. In these systems, the non-trivial dynamics associated with leg recirculation significantly affects the motion of the torso [17]. To generate periodic bounding motions in quadrupedal models with non-negligible leg inertia and segmented torso, [5] used PID control loops to impose desired values on the relative angle between the two segments of the torso and the leg touchdown angles. Optimization based on a modified version of the specific resistance that favors speed over efficiency resulted in bounding motions that require considerable power input since no energy storage elements have been considered. A similar model was used in [14] to search for high-performance bounding motions with low energy consumption. The spinal and hip joints were controlled in an open-loop fashion via central pattern generators and the generated motions were not necessarily stable. In a different vein, [11] combined swing-leg retraction with stance-leg impedance control to produce stable bounding; albeit powerful, this method relies on sufficiently actuated legs, and the presence of compliant elements in the leg's structure may require non-trivial modifications.

In this work, we take advantage of our previous results in [2, 3] to develop a control law that combines energy efficient motions with stability in a model with flexible torso

This work is supported by NSF grant IIS-135072 and ARL contract W911NF-12-1-0117.

Qu Cao and Ioannis Poulakakis
Department of Mechanical Engineering, University of Delaware, Newark, DE, USA. E-mail: caoqu@udel.edu, poulakas@udel.edu

and compliant legs that feature non-negligible inertia. The proposed controller generates cyclic bounding motions by merely actuating the hip joints to place the legs during flight; *no* control effort is exerted at the hip of a leg in contact with the ground. As a result, bounding is generated naturally, through the interaction between the torso's and legs' passive compliant elements and the environment. To ensure stability, the controller is augmented with an additional component that actively coordinates the torso's flexion-extension oscillation with the motion of the support leg during the stance phases, and updates the leg touchdown angles in a step-by-step fashion during the flight phases.

Another aspect investigated in this work is the regulation of forward velocity. A variety of controllers has been proposed to adjust running speed; these controllers typically modify hip torques during stance or touchdown angles during flight [10, 16, 21]. A different approach has been proposed in [11], where galloping motions over a wide range of running speeds have been generated by "shaping" the vertical ground reaction forces through the hip and knee joint torques. However, the requirement of sufficiently actuated legs may restrict this method to models without springy legs. By way of contrast, this work formulates speed control as a gait transition problem [4]. A switching controller is employed to pass from a "source" bounding motion to "target" one at the desired running speed, provided that the fixed point associated with the "source" gait is in the domain of attraction of the fixed point associated with the "target" gait. In this paper, estimates of the domains of attraction of the fixed points involved in speed transitions are computed as sub-level sets of quadratic Lyapunov functions that are verified through sums-of-squares programming as in [20].

2 Model and Gait Assumptions

The sagittal-plane quadrupedal model studied in this work is depicted in Fig. 1. The torso consists of two identical rigid bodies – one represents the posterior and the other the anterior part – connected through a torsional spring. Both the anterior and the posterior legs have the same structure; an upper segment with mass and inertia and a lower segment represented by a massless spring. The interaction between the toe and the ground is modeled as an unactuated, frictionless pin joint. The physical parameters of the model are shown in Table 1.

We consider the bounding gait depicted in Fig. 2. Depending on the state of the legs and the configuration of the torso, the bounding cycle can be divided into four phases: stance-posterior (sp), stance-anterior (sa), flight-gathered (fg) and flight-extended (fe). These phases are separated by liftoff and touchdown events. Note that in the gathered flight, the torso assumes a concave configuration, while in the extended flight it assumes a convex configuration.

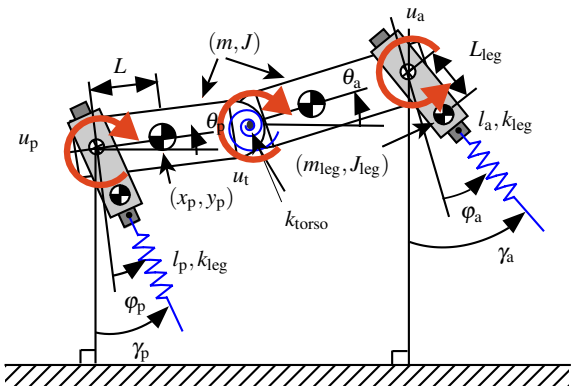

Fig. 1 The sagittal-plane quadrupedal model with a flexible torso and non-trivial leg mass.

Table 1 Mechanical Parameters of the Model

Parameter	Value	Units
Half Torso Mass (m)	10.432	kg
Half Torso Inertia (J)	0.36	kgm^2
Hip-to-COM Spacing (L)	0.138	m
Nominal Leg Length (l_0)	0.36	m
Leg Spring Constant (k_{leg})	7329	N/m
Torso Spring Constant (k_{torso})	203	Nm/rad
Leg Mass (m_{leg})	1	kg
Leg Inertia (I_{leg})	0.001	kgm^2
Hip-to-Leg COM Spacing (L_{Leg})	0.09	m

3 Hybrid Dynamics of Bounding

With reference to Fig. 1, in the stance phases $i \in \{\text{sp}, \text{sa}\}$, the configuration space Q_i can be parameterized by the length of the leg in contact with the ground – that is, $l_p \in \mathbb{R}$ for the posterior and $l_a \in \mathbb{R}$ for the anterior stance phase – the leg angles $(\varphi_p, \varphi_a) \in \mathbb{S}^2$ relative to the torso, and the pitch angles of the two segments of the torso – namely, $(\theta_p, \theta_a) \in \mathbb{S}^2$; i.e.,

$$q_i := \begin{cases} (l_p, \varphi_p, \varphi_a, \theta_p, \theta_a)' \in Q_i \text{ for } i = \text{sp} \ , \\ (l_a, \varphi_p, \varphi_a, \theta_p, \theta_a)' \in Q_i \text{ for } i = \text{sa} \ . \end{cases} \tag{1}$$

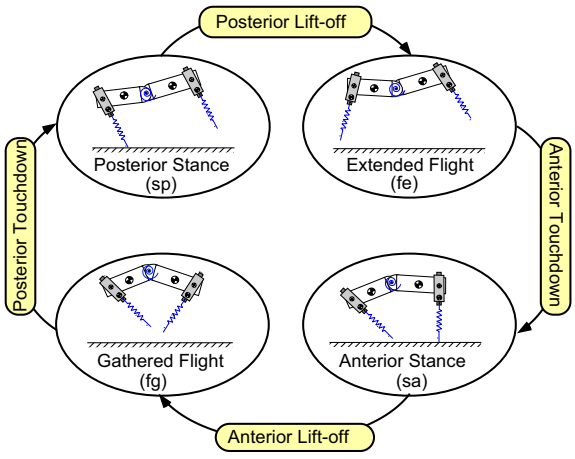

Fig. 2 Bounding phases and events.

In the flight phases, the configuration space Q_i, $i \in \{\text{fg},\text{fe}\}$, can be parameterized by the Cartesian coordinates $(x_\text{p}, y_\text{p}) \in \mathbb{R}^2$ of the COM of the posterior part of the torso, the pitch angles $(\theta_\text{p}, \theta_\text{a}) \in \mathbb{S}^2$ of the posterior and anterior parts of the torso, together with the leg angles $(\varphi_\text{p}, \varphi_\text{a}) \in \mathbb{S}^2$; i.e,

$$q_i := (x_\text{p}, y_\text{p}, \varphi_\text{p}, \varphi_\text{a}, \theta_\text{p}, \theta_\text{a})' \in Q_i \ \text{ for } \ i \in \{\text{fg},\text{fe}\} \ . \tag{2}$$

The equations that govern the motion of the model in all phases can be derived using the method of Lagrange, and are written in state-space form as

$$\begin{aligned} \dot{x}_i &= f_i(x_i) + g_i(x_i)u_i \\ &= f_i(x_i) + g_i^\text{a}(x_i)u_i^\text{a} + g_i^\text{p}(x_i)u_i^\text{p} + g_i^\text{t}(x_i)u_i^\text{t} \end{aligned} \tag{3}$$

where $x_i := (q_i',\ \dot{q}_i')'$ is the state vector for each phase $i \in \{\text{sp},\text{sa},\text{fg},\text{fe}\}$ evolving in $TQ_i := \{(q_i',\ \dot{q}_i')' |\ q_i \in Q_i,\ \dot{q}_i \in \mathbb{R}^{\dim(Q_i)}\}$. The input $u_i := (u_i^\text{p}, u_i^\text{a}, u_i^\text{t})'$ includes the torques applied at the posterior hip joint, the anterior hip joint and the torso joint, respectively.

The continuous-time phases are separated by discrete events. The flight phases terminate when the vertical distance between the toe of either the posterior or the anterior leg and the ground becomes zero. Due to the non-negligible mass of the upper leg, an impact occurs at touchdown which is modeled as in [3]. On the other hand, transitions from stance to flight occur when the vertical ground reaction force reduces to zero.

4 Generating Periodic Motions: Leg Recirculation

The objective of this section is to generate periodic bounding motions in the model of Fig. 1. Although periodic bounding motions cannot be generated passively as in [1, 2] due to the non-trivial leg mass and inertia, we can still take advantage of the passive dynamics associated with the torso and leg springs in exciting periodic motions. That is, in generating bounding motions, the torso joint is kept unactuated throughout the phases, i.e., $u_i^\text{t} = 0$ for $i \in \{\text{sp},\text{sa},\text{fe},\text{fg}\}$, while the hip joint is actuated *only* when the corresponding leg is in flight so that the controller merely swings the leg forward to the desired touchdown angle.

To design the controller, we begin by associating an output function of the form

$$y_i = q_{\text{c},i} - h_i^\text{d1}(s_i(q_i), \alpha_i, \beta_i) \ , \tag{4}$$

to the dynamics (3), where $i \in \{\text{sa},\text{fg},\text{sp},\text{fe}\}$. In (4), $q_{\text{c},i}$ includes the controlled variables and h_i^d1 represents their desired evolution, which is parameterized via a set of parameters α_i and β_i as detailed below. The controlled variables $q_{\text{c},i}$ are different for each phase; in more detail,

$$q_{\text{c},i} := \begin{cases} \gamma_\text{p} = \varphi_\text{p} + \theta_\text{p} & \text{for } \ i = \text{sa}, \\ \gamma_\text{a} = \varphi_\text{a} + \theta_\text{a} & \text{for } \ i = \text{sp}, \\ (\gamma_\text{p}, \gamma_\text{a})' & \text{for } \ i \in \{\text{fe},\text{fg}\} \ . \end{cases} \tag{5}$$

In (4), $s_i \in [0,1]$ is a monotonically increasing quantity defined as $s_i := (x_{\text{p},i}^\text{max} - x_\text{p})/x_{\text{p},i}^\text{max}$, where $x_{\text{p},i}^\text{max}$ is the travelled distance of the COM of the posterior torso in each phase. Note that the output y_i in (4) is specified by a function that depends only on the configuration variables q_i, and thus can be interpreted as a holonomic constraint imposed on the system via the hip actuators as described below.

4.1 Designing the constraints

Posterior Stance: As was mentioned above, during the posterior stance phase, the hip joint of the leg in contact with the ground is unactuated $u_\text{sp}^\text{p} = 0$, and the only input acting on the system is applied at the hip of the anterior leg with the objective of placing the anterior leg at a desired touchdown angle. Hence, the dynamics (3) can be simplified as

$$\dot{x}_\text{sp} = f_\text{sp}(x_\text{sp}) + g_\text{sp}^\text{a}(x_\text{sp})u_\text{sp}^\text{a} \ . \tag{6}$$

The desired evolution h_sp^d1 of the absolute anterior leg angle is parameterized via a 3rd-order Beziér polynomial with coefficients $\alpha_\text{sp} := \{\alpha_{\text{sp},k}\}_{k=0,1}$ and $\beta_\text{sp} := \{\beta_{\text{sp},k}\}_{k=0,1}$; i.e.,

$$\begin{aligned} h_\text{sp}^\text{d1}(s_\text{sp}(q_\text{sp}), \alpha_\text{sp}, \beta_\text{sp}) &= \sum_{k=0}^{1} b_{\text{sp},k}(s_\text{sp}(q_\text{sp}))\alpha_{\text{sp},k} \\ &+ b_{\text{sp},2}(s_\text{sp}(q_\text{sp}))\beta_{\text{sp},0} + b_{\text{sp},3}(s_\text{sp}(q_\text{sp}))\beta_{\text{sp},1} \ , \end{aligned} \tag{7}$$

where the terms $b_{\text{sp},k}$ are given by

$$b_{\text{sp},k}(s_\text{sp}) := \frac{3!}{k!(3-k)!} s_\text{sp}^k (1 - s_\text{sp})^{3-k} \ . \tag{8}$$

By properties of Beziér polynomials [22], $h_\text{sp}^\text{d1}(1) = \beta_{\text{sp},1}$ and $\partial h_\text{sp}^\text{d1}/\partial s_\text{sp}|_{s_\text{sp}=1} = 3(\beta_{\text{sp},1} - \beta_{\text{sp},0})$. Hence, selecting $\beta_{\text{sp},0} = \beta_{\text{sp},1}$ results in bounding gaits in which the anterior leg touches down at an angle $\beta_{\text{sp},1}$ with zero angular velocity.

Extended Flight: During the extended flight, the posterior leg swings forward while the anterior leg maintains a constant angle $\beta_{\text{sp},1}$ in anticipation of touchdown. The corresponding hip torques u_sa^p and u_sa^a are both available for control, and the desired evolution in (4) is defined as

$$h_\text{fe}^\text{d1}(s_\text{fe}(q_\text{fe}), \alpha_\text{fe}) = \begin{bmatrix} \sum_{k=0}^{3} b_{\text{fe},k}(s_\text{fe}(q_\text{fe}))\alpha_{\text{fe},k} \\ \beta_{\text{sp},1} \end{bmatrix}, \tag{9}$$

where α_fe includes the Beziér polynomial coefficients and b_fe is determined in a way analogous to (8).

Anterior Stance: During the anterior stance phase, the leg in contact with the ground is unactuated $u_\text{sa}^\text{a} = 0$, so that

$$\dot{x}_\text{sa} = f_\text{sa}(x_\text{sa}) + g_\text{sa}^\text{p}(x_\text{sa})u_\text{sa}^\text{p} \ . \tag{10}$$

The desired evolution of the posterior leg angle is

$$\begin{aligned} h_\text{sa}^\text{d1}(s_\text{sa}(q_\text{sa}), \alpha_\text{sa}, \beta_\text{sa}) &= \sum_{k=0}^{1} b_{\text{sa},k}(s_\text{sa}(q_\text{sa}))\alpha_{\text{sa},k} \\ &+ b_{\text{sa},2}(s_\text{sa}(q_\text{sa}))\beta_{\text{sa},0} + b_{\text{sa},3}(s_\text{sa}(q_\text{sa}))\beta_{\text{sa},1} \ . \end{aligned} \tag{11}$$

Again, we set $\beta_{\text{sa},0} = \beta_{\text{sa},1}$ so that the posterior leg arrives at the angle $\beta_{\text{sa},1}$ with zero angular velocity at the end of the anterior stance.

Gathered Flight: Similarly to the extended flight phase, in the gathered flight phase, the posterior leg maintains a constant angle while the anterior leg evolves according to

$$h_{\text{fg}}^{\text{d1}}(s_{\text{fg}}(q_{\text{fg}}),\alpha_{\text{fg}}) = \begin{bmatrix} \beta_{\text{sa},1} \\ \sum_{k=0}^{3} b_{\text{fg},k}(s_{\text{fg}}(q_{\text{fg}}))\alpha_{\text{fg},k} \end{bmatrix}. \tag{12}$$

4.2 Imposing the constraints

To impose the constraints (4) on the dynamics (3) we differentiate (4) twice with respect to time to obtain

$$\begin{aligned} \frac{d^2 y_i}{dt^2} &= L_{f_i}^2 y_i(x_i,\alpha_i,\beta_i) + L_{g_i^{\text{a}}} L_{f_i} y_i(q_i,\alpha_i,\beta_i) u_i^{\text{a}} \\ &\quad + L_{g_i^{\text{p}}} L_{f_i} y_i(q_i,\alpha_i,\beta_i) u_i^{\text{p}} \ , \end{aligned} \tag{13}$$

where $L_{f_i}^2 y_i$, $L_{g_i^{\text{a}}} L_{f_i} y_i$ and $L_{g_i^{\text{p}}} L_{f_i} y_i$ are the Lie derivatives of the output function y_i defined by (4) along the vector fields f_i, g_i^{a} and g_i^{p} that participate in (3). In each phase, the inputs available – i.e., $(u_i^{\text{p}}, u_i^{\text{a}})$ in the gathered and extended flight phases, u_i^{p} in the anterior stance and u_i^{a} in the posterior stance – are selected to ensure $d^2 y_i/dt^2 = 0$. This can be done by following standard procedures as in [22, Chapter 5]; the details are not included here due to space limitations.

4.3 Poincaré map and local stability

The dynamics of bounding can be described by concatenating the continuous-time phases according to the sequence of Fig. 2. To study the existence of periodic motions, the method of Poincaré is used with the Poincaré section taken right after the anterior leg liftoff; i.e.,

$$\mathscr{S} := \{x_{\text{fg}} \in TQ_{\text{fg}} \mid y_{\text{p}} - y_{\text{p}}^* = 0\} \ , \tag{14}$$

where $y_{\text{p}}^* = l_0 \cos(\theta_{\text{a}} + \varphi_{\text{a}}) + 2L\cos\theta_{\text{a}} - L\cos\theta_{\text{p}}$. By projecting out the monotonically increasing horizontal coordinate x_{p} from the state vector x_{fg} and substituting y_{p} through the condition defining (14), the Poincaré map can be defined as

$$z[k+1] = P_1(z[k],\alpha[k],\beta[k]) \ , \tag{15}$$

where z represents the remaining states in x_{fg}, i.e.,

$$z := (\theta_{\text{p}}, \theta_{\text{a}}, \varphi_{\text{p}}, \varphi_{\text{a}}, \dot{x}_{\text{p}}, \dot{y}_{\text{p}}, \dot{\theta}_{\text{p}}, \dot{\theta}_{\text{a}}, \dot{\varphi}_{\text{p}}, \dot{\varphi}_{\text{a}})' \ , \tag{16}$$

and the arrays $\alpha = \{\alpha_i, x_{\text{p},i}^{\max}, x_{\text{p},i}^{\min}\}$, $i \in \{\text{sp}, \text{sa}, \text{fe}, \text{fg}\}$ and $\beta = \{\beta_{\text{sa}}, \beta_{\text{sp}}\}$ include all the parameters introduced by the leg recirculation controller. Given the Poincaré map defined in (15), the problem of computing periodic bounding gaits becomes equivalent to finding a state vector z so that $z = P_1(z,\alpha,\beta)$ for suitable parameter values α and β, and can be solved numerically using MATLAB's `fmincon`.

Figure 3 shows the evolution of forward velocity x_{p}, torso oscillation $\theta_{\text{a}} - \theta_{\text{p}}$, absolute leg angles $(\gamma_{\text{p}}, \gamma_{\text{a}})$ and the hip torque input $(u^{\text{p}}, u^{\text{a}})$ of a representative fixed point. Note that in Fig. 3(b) there is one torso flexion-extension oscillation in one stride, as in the passively generated bounding motions of [1]. Also, the maximum and minimum torso angle occur in the extended and gathered flight phases, corresponding to the convex and concave configurations, respectively.

Finally, to analyze local stability of the computed bounding motions, we linearize (15) at a fixed point $\bar{z}$ assuming α and β are constants. The corresponding linearized system is

$$\Delta z[k+1] = A_1 \Delta z[k] \ , \tag{17}$$

where $\Delta z = z - \bar{z}$ and $A_1 = \partial P_1/\partial z|_{z=\bar{z},\ \alpha=\bar{\alpha},\ \beta=\bar{\beta}}$. When the eigenvalues of A_1 lie within the unit disc, the corresponding fixed point is locally exponentially stable. However, the fixed points generated based on the leg recirculation controller are not stable, and additional control action is necessary to sustain periodic bounding orbits in the presence of perturbations.

5 Stabilizing Periodic Motions: Leg-torso Coordination

The control approach adopted here to stabilize the bounding motions generated with the leg recirculation controller of Section 4 is similar to the one proposed in [2]. First, an active torque u_i^{t} acting *in parallel* with the torsional spring connecting the two parts of the torso is introduced. Then, u_i^{t} is used to influence the coordination between the torso's flexion-extension oscillations and the motion of the legs.

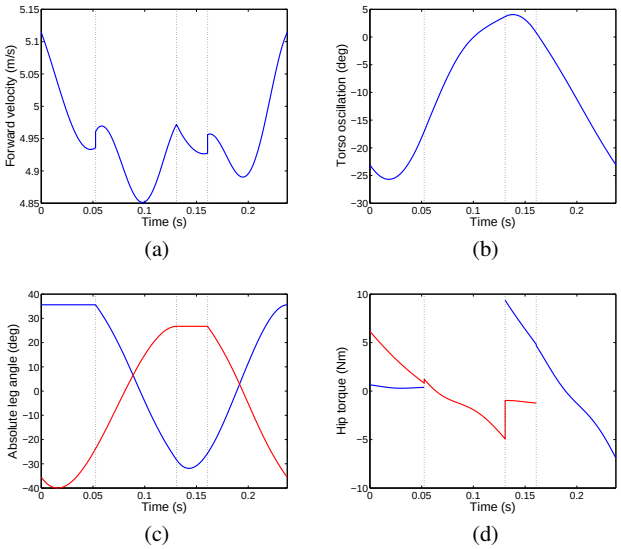

Fig. 3 Evolution of forward velocity (a), torso oscillation (b), absolute leg angles (c) and hip joint torque (d) of a fixed point. In (c) and (d), the red and blue lines correspond to the anterior and posterior legs, respectively. The vertical lines separate one cycle into four phases: from left to right, fg, sp, fe and sa. The discontinuities are due to the impact at touchdown.

5.1 Continuous-time control

With the introduction of the input u_i^{t}, the system (3) in *closed loop* with the corresponding action of the leg recirculation controller of Section 4 takes the form

$$\dot{x}_i = f_i^{\mathrm{cl}}(x_i) + g_i^{\mathrm{t}}(x_i)u_i^{\mathrm{t}} \ . \tag{18}$$

For the stance phases $i \in \{\mathrm{sp}, \mathrm{sa}\}$ consider the output

$$y_i = (\theta_{\mathrm{a}} - \theta_{\mathrm{p}}) - h_i^{\mathrm{d2}}(\varsigma_i(q_i), \eta_i) \ , \tag{19}$$

where h_i^{d2} is the desired output of the relative pitch angle $\theta_{\mathrm{a}} - \theta_{\mathrm{p}}$. It is through h_i^{d2} that the information about the leg-torso coordination pattern is passed to the feedback controller. In more detail, given a desired cyclic bounding gait generated by the leg recirculation controller of Section 4, h_i^{d2} is designed by fitting a suitably parameterized polynomial on the evolution of the relative pitch angle $(\theta_{\mathrm{a}} - \theta_{\mathrm{p}})$ as a function of the corresponding support leg angle; i.e.,

$$h_i^{\mathrm{d2}}(\varsigma_i(q_i)) = \sum_{k=0}^{3} c_{i,k}(\varsigma_i(q_i))\eta_{i,k} \ , \tag{20}$$

where $\eta_{i,k}$ are polynomial coefficients, $c_{i,k}$ are given by

$$c_{i,k}(\varsigma_i) := \frac{3!}{k!(3-k)!}\varsigma_i^k(1-\varsigma_i)^{3-k} \ , \tag{21}$$

and ς_i, $i \in \{\mathrm{sp}, \mathrm{sa}\}$, are the strictly monotonic quantities

$$\varsigma_{\mathrm{sa}} := \frac{\gamma_{\mathrm{a}}^{\max} - \gamma_{\mathrm{a}}}{\gamma_{\mathrm{a}}^{\max} - \gamma_{\mathrm{a}}^{\min}} \quad \text{and} \quad \varsigma_{\mathrm{sp}} := \frac{\gamma_{\mathrm{p}}^{\max} - \gamma_{\mathrm{p}}}{\gamma_{\mathrm{p}}^{\max} - \gamma_{\mathrm{p}}^{\min}} \ ,$$

in which $\gamma_{\mathrm{a}}^{\max}$ and $\gamma_{\mathrm{a}}^{\min}$ are the maximum and minimum values of γ_{a} and similarly $\gamma_{\mathrm{p}}^{\max}$ and $\gamma_{\mathrm{p}}^{\min}$ are the corresponding values for γ_{p}. Hence, in a way analogous to [2], (20) effectively "slaves" the torso's motion during the stance phases so that its evolution is determined by the absolute angle of the corresponding leg that is in contact with the ground. As in Section 4.2, selecting

$$u_i^{\mathrm{t}} = -(L_{g_i^{\mathrm{t}}}L_{f_i^{\mathrm{cl}}}y_i)^{-1}L_{f_i^{\mathrm{cl}}}^2 y_i(x_i) \ , \tag{22}$$

where $L_{g_i^{\mathrm{t}}}L_{f_i^{\mathrm{cl}}}y_i$ and $L_{f_i^{\mathrm{cl}}}^2 y_i$ are the Lie derivatives of (19) along the vector fields f_i^{cl}, g_i^{t} of (18) results in $d^2y_i/dt^2 = 0$.

Adopting $\mathscr{S}$ of (14) as the Poincaré section, the corresponding Poincaré map is defined as

$$z[k+1] = P_2(z[k], \alpha[k], \beta[k], \eta[k]) \tag{23}$$

where $\eta = \{\eta_{\mathrm{sa}}, \eta_{\mathrm{sp}}, \gamma_{\mathrm{p}}^{\max}, \gamma_{\mathrm{a}}^{\max}, \gamma_{\mathrm{p}}^{\min}, \gamma_{\mathrm{a}}^{\min}\}$, and α and β are the parameters introduced by the leg recirculation controller of Section 4. Due to the error introduced by fitting the polynomial (20) on the evolution of $(\theta_{\mathrm{a}} - \theta_{\mathrm{p}})$ corresponding to a fixed point computed in Section 4, a new fixed point must be computed by requiring that $z = P_2(z, \alpha, \beta, \eta)$ and new nominal values for the parameters α, β and η are determined. Note that because the fitting errors are small, the computation of a fixed point for (23) using a fixed point of (15) as an initial guess does not involve many iterations, and the two motions are in general very close.

Finally, to establish attractivity [22], the input (22) is augmented with an auxiliary control action ν as

$$u_i^{\mathrm{t}} = (L_{g_i^{\mathrm{t}}}L_{f_i^{\mathrm{cl}}}y_i)^{-1}[\nu(y_i, \dot{y}_i, \varepsilon) - L_{f_i^{\mathrm{cl}}}^2 y_i(x_i)] \tag{24}$$

where $\nu = -\frac{1}{\varepsilon^2}K_{\mathrm{P}}y_i - \frac{1}{\varepsilon}K_{\mathrm{V}}\dot{y}_i$, $K_{\mathrm{P}} > 0, K_{\mathrm{V}} > 0$ and $\varepsilon > 0$.

5.2 Discrete-time control

By the construction of the leg recirculation controller of Section 4, the parameter array β in (23) includes the absolute leg angles at touchdown. These angles (partially) determine when the corresponding gathered and extended flight phases are terminated, and are powerful control inputs available in discrete time. A variety of control procedures is available for updating the leg touchdown angles in an event-based fashion to enhance stability; see [16] or [19] for examples. Here, a discrete Linear Quadratic Regulator (LQR) is employed that positions the legs during flight based on feedback of the states at the Poincaré section $\mathscr{S}$ defined in (14). In what follows, the parameters α and η in (23) are kept constant and equal to their nominal values, while $\beta[k]$ will be updated in a step-by-step fashion. To emphasize that $\beta[k]$ is a discrete-time control input we write (with slight abuse of notation)

$$z[k+1] = P_2(z[k], \beta[k]) \ . \tag{25}$$

Linearizing (25) at a fixed point $\bar{z}$ of (23) results in

$$\Delta z[k+1] = A_2\Delta z[k] + B_2\Delta\beta[k] \tag{26}$$

where $\Delta z = z - \bar{z}$, $\Delta\beta = \beta - \bar{\beta}$, $A_2 = \partial P_2/\partial z|_{z=\bar{z},\beta=\bar{\beta}}$ and $B_2 = \partial P_2/\partial\beta|_{z=\bar{z},\beta=\bar{\beta}}$. Define the cost function

$$J(\Delta z) = \sum_{i=k}^{\infty}(\Delta z' Q\Delta z + \Delta\beta' R\Delta\beta), \tag{27}$$

where $Q = Q' \geq 0, R = R' > 0$. It can be shown – see [20] and references therein – that the optimal cost-to-go J^* is

$$J^*(\Delta z) = \Delta z' S\Delta z, \quad S' = S > 0 \tag{28}$$

where S is the solution of the associated discrete-time Riccati equation. The optimal feedback policy updates the swing-leg touchdown angles according to

$$\Delta\beta[k] = -K\Delta z[k] \ . \tag{29}$$

where K is derived from S as $K = (B_2'SB_2 + R)^{-1}(B_2'SA_2)$, and K and S are given by MATLAB's `dlqr`. With the controller (29), the closed-loop return map becomes

$$z[k+1] = P_2(z[k], \bar{\beta} - K\Delta z[k]) := P_3(z[k]) \ , \tag{30}$$

and all the eigenvalues of the Jacobian $\partial P_3/\partial z|_{z=\bar{z}}$ are located within the unit disc. To illustrate the orbit's local stability, the state prior to liftoff of the bounding motion in Fig. 3 is perturbed away from the fixed point by an initial error of $+0.1\text{m/s}$ in $\dot{x}_\text{p}$ and -3deg in θ_a. The system converges back to the nominal motion as shown in Fig. 4. Note that the toe/ground interaction constraints are respected and the maximum torso torque is less than 40Nm.

6 Speed Transitions

In this work, speed transitions will be realized by switching between stable limit cycles according to the idea presented in Fig. 5. In the setting of Fig. 5, the limit cycles ϕ_0 and ϕ_1 represent periodic bounding motions at different running speeds, the surfaces $\mathscr{S}_0$ and $\mathscr{S}_1$ denote suitable Poincaré sections and $\bar{z}_0$ and $\bar{z}_1$ are the corresponding fixed points. The domain of attraction of each of the fixed points $\bar{z}_0$ and $\bar{z}_1$ on $\mathscr{S}_0$ and $\mathscr{S}_1$ is denoted[1] by $\mathscr{D}_0$ and $\mathscr{D}_1$, respectively. By examining the relationship between the domains of attraction and the fixed points, the feasibility of generating a transition can be determined. For example, as shown in Fig. 5, if $\bar{z}_0 \in \mathscr{D}_1$, then employing a switching controller $\Gamma_{0\to1}$,

$$\Gamma_{0\to1}((\alpha_0,\beta_0,\eta_0,K_0)\to(\alpha_1,\beta_1,\eta_1,K_1)) \ , \tag{31}$$

which effectively changes the controller parameters from those corresponding to the orbit ϕ_0 to those of ϕ_1, resulting in the motion of the system being attracted by the target orbit ϕ_1. Symbolically: if $\bar{z}_0 \in \mathscr{D}_1$, then $\bar{z}_0 \xrightarrow{\Gamma_{0\to1}} \bar{z}_1$. Furthermore, if $\bar{z}_1 \in \mathscr{D}_0$, then two-way transitions can be realized enabling both acceleration and deceleration; such transitions will be denoted as $\bar{z}_0 \xleftrightarrow[\Gamma_{1\to0}]{\Gamma_{0\to1}} \bar{z}_1$.

Generally, determining the domain of attraction of an equilibrium point is a difficult task, even for low-dimensional systems. Yet, as detailed in the following section, for the ten-dimensional system (30), the domain of attraction of a bounding fixed point can be estimated as a sub-level set of a quadratic Lyapunov function [8] using sums-of-squares (SOS) verification [12, 20].

[1] Note that $\mathscr{D}_0$ and $\mathscr{D}_1$ do not represent the domains of attraction of the entire periodic orbits ϕ_0 and ϕ_1.

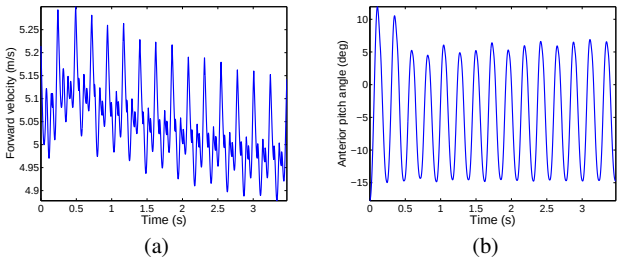

(a) (b)

Fig. 4 The evolution of the forward velocity and the anterior pitch when the system is perturbed with $+0.1\text{m/s}$ in $\dot{x}_\text{p}$ and -3deg in θ_a.

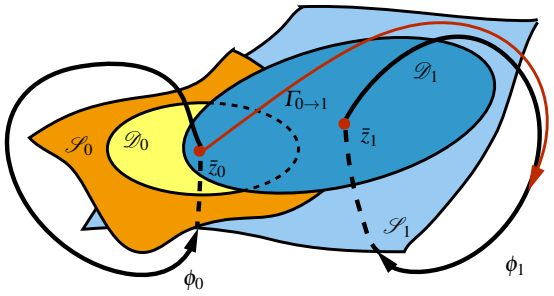

Fig. 5 A conceptual illustration of the transition between two limit cycles, i.e., ϕ_0 and ϕ_1. $\mathscr{S}_0$ and $\mathscr{S}_1$ are the Poincaré sections of ϕ_0 and ϕ_1, and $\bar{z}_0$ and $\bar{z}_1$ are the corresponding fixed points. $\mathscr{D}_0$ and $\mathscr{D}_1$ are the domain of attractions at the Poincaré sections for ϕ_0 and ϕ_1 respectively.

6.1 Estimating the domain of attraction

For ease of implementation, a fixed point $\bar{z}$ of (30) is translated to the origin. Let $\tilde{z}[k] = z[k] - \bar{z}$, then (30) implies

$$\tilde{z}[k+1] = P_3(\bar{z}+\tilde{z}[k]) - \bar{z} \ , \tag{32}$$

which represents a map from $\tilde{z}[k]$ to $\tilde{z}[k+1]$; i.e.,

$$\tilde{z}[k+1] = P_4(\tilde{z}[k]) \ . \tag{33}$$

The origin is a fixed point of (33), and its domain of attraction can be used to determine the domain of attraction of the corresponding fixed point $\bar{z}$ of (30).

A function $V(\tilde{z})$ is a Lyapunov function for the system (33) if $V(\tilde{z})$ is positive definite and $V(\tilde{z}[k+1]) - V(\tilde{z}[k]) < 0$ in a bounded domain $\mathscr{D}$; we consider domains of the form

$$\mathscr{D}(\rho) := \{\tilde{z} \mid 0 \le V(\tilde{z}) \le \rho\} \ , \tag{34}$$

where ρ is a positive scalar. Note that the linear optimal cost-to-go function (28) is already a Lyapunov function. Thus, by defining $V(\tilde{z}) := J^*(\tilde{z})$, the problem of estimating the domain of attraction takes the form

$$\begin{aligned} &\max \ \rho \\ &\text{s.t} \ \ \forall \tilde{z} \in \mathscr{D}(\rho), J^*_+(\tilde{z}[k]) < 0 \ , \end{aligned} \tag{35}$$

where $J^*_+(\tilde{z}[k]) = J^*(\tilde{z}[k+1]) - J^*(\tilde{z}[k])$.

One way to check that the Lyapunov function is decreasing within the domain $\mathscr{D}$ is to formulate a sums-of-squares (SOS) feasibility problem [12] as shown in [20]. A multivariate polynomial $h(x) := h(q_1,\ldots,q_n)$ is a sum of squares if there exist polynomials $f_1(x),\ldots,f_m(x)$ such that $h(x) = \sum_{i=1}^m f_i^2(x)$. This is equivalent to the existence of a positive semidefinite matrix H such that $h(x) = Z'(x)HZ(x)$, where $Z(x)$ is a suitably chosen vector of monomials. For a given polynomial, SOS programming checks the non-negativity of the polynomial h by searching for a positive semidefinite matrix H [12]. Then, (35) can be substituted by the

more conservative – but also more tractable – SOS feasibility problem, as follows

$$\begin{aligned} &\max \rho \\ &\text{s.t } h(\tilde{z}) \text{ is SOS} \ , \\ &-J_+^*(\tilde{z}[k]) - h(\tilde{z}[k])(\rho - J^*(\tilde{z}[k])) \text{ is SOS} \ , \end{aligned} \tag{36}$$

where $h(\Delta z)$, a positive definite polynomial of Δz. Note that the SOS algorithm requires $J_+^*(\tilde{z}[k])$ to be a polynomial [15]. However, in our case,

$$\begin{aligned} J_+^*(\tilde{z}[k]) &= \tilde{z}'[k+1] S \tilde{z}[k+1] - \tilde{z}'[k] S \tilde{z}[k] \\ &= P_4(\tilde{z}[k])' S P_4(\tilde{z}[k]) - \tilde{z}'[k] S \tilde{z}[k] \ , \end{aligned} \tag{37}$$

in which $P_4(\tilde{z}[k])$ is not available in closed form; it is obtained through numerical integration. Hence, to proceed with the method, we approximate the return map (33) by expanding P_4 in Taylor series keeping terms up to second order:

$$P_4(\tilde{z}[k]) \approx T_1 \tilde{z}[k] + \tilde{z}'[k] T_2 \tilde{z}[k] \ , \tag{38}$$

where $T_1 = \left.\dfrac{\partial P_4}{\partial \tilde{z}_i}\right|_{\tilde{z}=0}$, $T_2 = \dfrac{1}{2}\left.\dfrac{\partial^2 P_4}{\partial \tilde{z}_i \partial \tilde{z}_j}\right|_{\tilde{z}=0}$,

for $i, j \in \{1, 2, ..., 10\}$. Substituting (38) into (37) yields

$$\begin{aligned} J_+^*(\tilde{z}[k]) = &\left(T_1 \tilde{z}[k] + \tilde{z}'[k] T_2 \tilde{z}[k]\right)' S \left(T_1 \tilde{z}[k] + \tilde{z}'[k] T_2 \tilde{z}[k]\right) \\ &- \tilde{z}'[k] S \tilde{z}[k] \ . \end{aligned} \tag{39}$$

Given the polynomial expression (39), the SOS feasibility program in (36) can be solved by any available SOS toolbox, such as SOSTOOLS [15], and the maximum value $\rho^{\max}$ can be determined by a binary search for the value of ρ above which the SOS feasibility problem fails.

To provide some intuition on the conservativism associated with estimating the domain of attraction through the SOS method, we compare the maximum perturbation that can be accommodated by perturbing each state separately with the one predicted by the SOS estimate. Given $\rho^{\max}$, the largest tolerable single perturbation can be computed as $\Delta z^{\max}(i) = \sqrt{\rho^{\max}/S(i,i)}$ for $i = 1, 2, ...10$. For the fixed point in Fig. 4, $\Delta z^{\max} = (0.03, 0.03, 0.30, 0.04, 0.15, 0.13, 0.31, 0.37, 0.91, 0.90)$. Fig. 6 shows the ratio of these values to the values obtained from simulation by regarding a perturbation as tolerable if the error in the sates is less that 5% after 15 strides. It can be seen from Fig. 6 that the ratio is diverse among different states. For instance, in the positive direction of φ_a, the SOS method can only capture less than 20% of the value that can be accommodated. On the other hand, in the negative direction of $\dot{y}_p$, more than 90% can be captured by $\Delta z^{\max}$, indicating that $\rho^{\max}$ is constrained by the capability of the system to deal with negative disturbances in $\dot{y}_p$. This observation is consistent with our previous studies in [2], implying that perturbations that tend to decrease hopping height are more critical, since they are more likely to result in toe stubbing and failure to run due to the lack of active control over leg length.

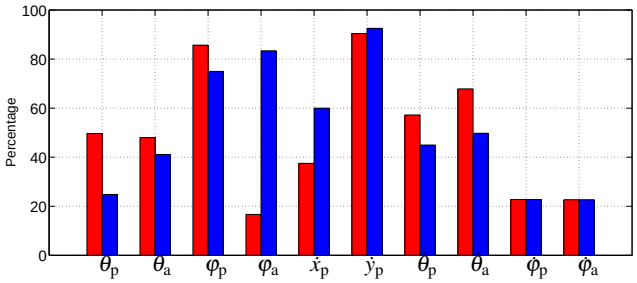

Fig. 6 Ratio of the largest single perturbation that can be tolerated as is predicted by the SOS method over the corresponding value obtained by numerical simulation. The red and blue bars correspond to the positive and negative perturbations, respectively.

6.2 Realizing speed transitions

In this section, we illustrate the procedure in the context of transitioning between fixed points at different running speeds. As shown in Fig. 7, the fixed point $\bar{z}_0$ is computed and its domain of attraction $\mathscr{D}_0$ is estimated. Because the estimate of the domain of attraction lies in a high dimensional state space, Fig. 7 only shows its projection on the $(\dot{x}_p, \dot{y}_p)$ plane. The fixed points $\bar{z}_1$ and $\bar{z}_2$ are both located within $\mathscr{D}_0$, and have been computed by adding an inequality constraint when searching for them that characterizes their "distance" from $\bar{z}_0$; namely, $(\bar{z}_i - \bar{z}_0)' S_0 (\bar{z}_i - \bar{z}_0) \leq \rho_0^{\max}$ for $i \in \{1, 2\}$. The forward running speed of $\bar{z}_1$ is 5.9m/s and of $\bar{z}_2$ is 5.5m/s. After estimating the domains of attraction $\mathscr{D}_1$ of $\bar{z}_1$ and $\mathscr{D}_2$ of $\bar{z}_2$, transitions between the fixed points can be easily realized. First, since $\bar{z}_1, \bar{z}_2 \in \mathscr{D}_0$, then the transitions $\bar{z}_1 \xrightarrow{\Gamma_{1\to0}} \bar{z}_0$ and $\bar{z}_2 \xrightarrow{\Gamma_{2\to0}} \bar{z}_0$ are both feasible; these transitions are represented by the blue solid lines in Fig. 7. Reversely, $\bar{z}_0 \xrightarrow{\Gamma_{0\to1}} \bar{z}_1$ can be realized, as the green solid line in Fig. 7 shows, while $\bar{z}_0 \xrightarrow{\Gamma_{0\to2}} \bar{z}_2$ is not possible since $\bar{z}_0 \notin \mathscr{D}_1$. To realize the transition from $\bar{z}_0$ to $\bar{z}_2$, an intermediate fixed point can be computed which is in the domain of attraction of $\bar{z}_2$ and its domain of attraction includes $\bar{z}_0$.

By concatenating the basic transitions described above, multi-hop transitions can be realized between fixed points that are further apart, *provided* that each transition is given sufficient time to be completed. For example, a transition from $\bar{z}_2$ to $\bar{z}_1$ can be achieved using $\bar{z}_0$ as a "bridge" (that is, $\bar{z}_2 \xrightarrow{\Gamma_{2\to0}} \bar{z}_0 \xrightarrow{\Gamma_{0\to1}} \bar{z}_1$) corresponding to an increase in the running speed from 5.5m/s to 5.9m/s. It should be mentioned that the duration of a transition can be reduced by tracking the "distance" to the "target" fixed point. For example, in switching from $\bar{z}_2$ to $\bar{z}_1$, if the states enter the domain of attraction of $\bar{z}_1$ before converging to $\bar{z}_0$, then the switching controller will adopt the controller parameters of $\bar{z}_1$ in advance, and the evolution of the states will follow the dotted red line without spending time to first converge to $\bar{z}_0$. More generally, the transition dynamics can be modeled via a switching system as in [9], and less conservative conditions on switching can be obtained.

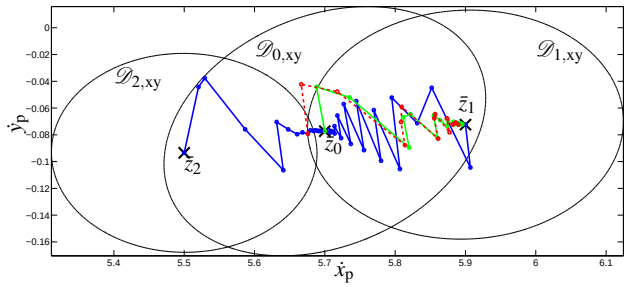

Fig. 7 Feasible transitions among fixed points $\bar{z}_0$, $\bar{z}_1$ and $\bar{z}_2$, each corresponding to a different running speed. For illustration, $\mathscr{D}_{0,\mathrm{xy}}$, $\mathscr{D}_{1,\mathrm{xy}}$ and $\mathscr{D}_{2,\mathrm{xy}}$ are the projections of the estimated domains of attraction on the $(\dot{x}_\mathrm{p}, \dot{y}_\mathrm{p})$ plane when the fixed points are perturbed on this plane. The blue line represents the transition from $\bar{z}_1$ and $\bar{z}_2$ to $\bar{z}_0$, while the green line represents the transition from $\bar{z}_0$ to $\bar{z}_1$. The dotted red line represents a "shortcut" in transition from $\bar{z}_2$ to $\bar{z}_1$, which decreases the transition time by 28% from 7.2s to 5.2s.

Finally, on a practical note, much of the computation associated with the method can be performed off-line, and a library of suitable fixed points $\bar{z}$ can be generated, each characterized by the control parameters (α, β, η, K) and the corresponding domain of attraction (S, ρ). Transitions can then be realized on-line simply by switching the values of the controller parameters to those of the targeted fixed point, provided that feasibility is satisfied.

7 Conclusions

This paper proposed a hybrid control law for stabilizing periodic bounding gaits in a model that features a flexible torso and compliant legs with non-trivial inertia. Periodic motions were generated in a nearly passive fashion, merely by recirculating the legs during flight. Local stability was achieved by coordinating the torso oscillation with the leg movement and updating the touchdown angles in a step-by-step fashion. The resulting stable bounding motions were then used to transition between speeds by switching between the corresponding fixed points based on estimates of their domains of attraction verified through sums-of-squares programming.

References

1. Cao, Q., Poulakakis, I.: Passive quadrupedal bounding with a segmented flexible torso. In: Proceedings of the IEEE/RSJ International Conference on Intelligent Robots and Systems, pp. 2484–2489 (2012)
2. Cao, Q., Poulakakis, I.: Quadrupedal bounding with a segmented flexible torso: passive stability and feedback control. Bioinspiration & Biomimetics **8**(4), 046,007 (2013)
3. Cao, Q., Poulakakis, I.: On the energetics of quadrupedal running: predicting the metabolic cost of transport via a flexible-torso model. Bioinspiration & Biomimetics **10**(5), 056,008 (2015)
4. Cao, Q., van Rijn, A.T., Poulakakis, I.: On the control of gait transitions in quadrupedal running. In: Proceedings of the IEEE/RSJ International Conference on Intelligent Robots and Systems, pp. 5136 – 5141 (2015)
5. Culha, U., Saranli, U.: Quadrupedal bounding with an actuated spinal joint. In: Proceedings of the IEEE International Conference on Robotics and Automation, pp. 1392–1397 (2011)
6. Deng, Q., Wang, S., Xu, W., Mo, J., Liang, Q.: Quasi passive bounding of a quadruped model with articulated spine. Mechanism and Machine Theory **52**, 232–242 (2012)
7. Full, R., Koditschek, D.E.: Templates and anchors: Neuromechanical hypotheses of legged locomotion on land. Journal of Experimental Biology **202**, 3325–3332 (1999)
8. Khalil, H.K.: Nonlinear Systems, third edn. Prentice Hall, Upper Saddle River, NJ (2002)
9. Motahar, M.S., Veer, S., Poulakakis, I.: Composing limit cycles for motion planning of 3D bipedal walkers. In: IEEE Conference on Decision and Control (2016). Submitted
10. Papadopoulos, D., Buehler, M.: Stable Running in a Quadruped Robot with Compliant Legs. In: Proceedings of the IEEE International Conference on Robotics and Automation, pp. 444–449 (2000)
11. Park, H.W., Kim, S.: Quadrupedal galloping control for a wide range of speed via vertical impulse scaling. Bioinspiration & Biomimetics **10**(2), 025,003 (2015)
12. Parrilo, P.A.: Structured semidefinite programs and semialgebraic geometry methods in robustness and optimization. Ph.D. thesis, California Institute of Technology (2000)
13. Poulakakis, I., Papadopoulos, E.G., Buehler, M.: On the stability of the passive dynamics of quadrupedal running with a bounding gait. The International Journal of Robotics Research **25**(7), 669–687 (2006)
14. Pouya, S., Khodabakhsh, M., Spröwitz, A., Ijspeert, A.: Spinal joint compliance and actuation in a simulated bounding quadruped robot. Autonomous Robots pp. 1–16 (2016)
15. Prajna, S., Papachristodoulou, A., Seiler, P., Parrilo, P.A.: New developments in sum of squares optimization and SOSTOOLS. In: Proceedings of the American Control Conference, pp. 5606–5611 (2004)
16. Raibert, M.H.: Legged Robots that Balance. MIT Press, Cambridge, MA (1986)
17. Schmiedeler, J.P., Siston, R., Waldron, K.J.: The significance of leg mass in modeling quadrupedal running gaits. In: G. Bianchi, J.C. Guinot, C. Rzymkowski (eds.) ROMANSY 14: Theory and Practice of Robots and Manipulators, pp. 481–488. Springer, Vienna (2002)
18. Seipel, J.E.: Analytic-holistic two-segment model of quadruped back-bending in the sagittal plane. In: Proceedings of ASME Mechanisms and Robotics Conference, vol. 6, pp. 855–861 (2011)
19. Seyfarth, A., Geyer, H., Herr, H.: Swing leg retraction: A simple control model for stable running. Journal of Experimental Biology **206**, 2547–2555 (2003)
20. Tedrake, R., Manchester, I.R., Tobenkin, M., Roberts, J.W.: LQR-trees: Feedback motion planning via sums-of-squares verification. The International Journal of Robotics Research **29**(8), 1038–1052 (2010)
21. Wang, X., Li, M., Wang, P., Sun, L.: Running and turning control of a quadruped robot with compliant legs in bounding gait. In: Proceedings of the IEEE International Conference on Robotics and Automation, pp. 511–518 (2011)
22. Westervelt, E.R., Grizzle, J.W., Chevallereau, C., Choi, J.H., Morris, B.: Feedback Control of Dynamic Bipedal Robot Locomotion. Taylor & Francis/CRC Press (2007)
23. Yamasaki, R., Ambe, Y., Aoi, S., Matsuno, F.: Quadrupedal bounding with spring-damper body joint. In: Proceedings of IEEE/RSJ International Conference on Intelligent Robots and Systems, pp. 2345–2350 (2013)
24. Zhang, Z.G., Fukuoka, Y., Kimura, H.: Stable quadrupedal running based on a spring-loaded two-segment legged models. In: Proceedings of the IEEE International Conference on Robotics and Automation, vol. 3, pp. 2601–2606 (2005)